Identification of recurrent non-coding mutations in B-cell lymphoma using capture Hi-C

Short title: Recurrent non-coding mutations in B-cell lymphoma

Alex J. Cornish[1], Phuc H. Hoang[1,2], Sara E. Dobbins[1], Philip J. Law[1], Daniel Chubb[1], Giulia Orlando[1], Richard S. Houlston[1,2,*].

1. Division of Genetics and Epidemiology, The Institute of Cancer Research, London, UK.
2. Division of Molecular Pathology, The Institute of Cancer Research, London, UK.

* Correspondence: Richard S. Houlston; Tel: +44(0) 208 722 4175, Fax: +44(0) 208 722 4365, e-mail: Richard.Houlston@icr.ac.uk, Postal Address: The Institute of Cancer Research, 15 Cotswold Road, Sutton, London SM2 5NG, UK.

Article word count: 3,940

Abstract word count: 168

Number of figures: 6

Number of tables: 0

Number of references: 60

Published in:

Blood Advances 2019 3:21-32; doi: https://doi.org/10.1182/bloodadvances.2018026419

ABSTRACT

The identification of driver mutations is fundamental to understanding oncogenesis. While genes frequently mutated in B-cell lymphoma have been identified, the search for driver mutations has largely focused on the coding genome. Here we report an analysis of the non-coding genome using whole genome sequencing data from 117 B-cell lymphoma patients. Using promoter capture Hi-C data in naïve B-cells we define *cis*-regulatory elements, which represent an enriched subset of the non-coding genome in which to search for driver mutations. We identify regulatory regions whose mutation significantly alters gene expression, including copy number variation at *cis*-regulatory elements targeting *CD69*, *IGLL5* and *MMP14*, and single-nucleotide variants in a *cis*-regulatory element for *TPRG1*. Additionally, we demonstrate the commonality of pathways targeted by coding and non-coding mutations, exemplified by *MMP14*, which regulates Notch signaling, a pathway important in lymphomagenesis, and whose expression is associated with patient survival. This study provides an enhanced understanding of lymphomagenesis and demonstrates the advantages of employing chromosome conformation capture to decipher non-coding mutations relevant to cancer biology.

KEY POINTS

- Integration of B-cell lymphoma genomic data and capture Hi-C reveals recurrently mutated regulatory elements influencing gene expression.
- Expression of *MMP14,* which is targeted by a mutated *cis*-regulatory element, is associated with B-cell lymphoma patient survival.

INTRODUCTION

B-cell lymphoma comprise a heterogeneous group of cancers, with diverse etiologies, clinical behaviors and outcomes[1]. The different B-cell lymphoma resemble B cells at specific stages of differentiation[1], with diffuse large B-cell lymphoma (DLBCL) and follicular lymphoma (FL), accounting for around 43% and 17% of cases respectively[2].

The identification of driver mutations is fundamental to understanding oncogenesis and response to therapy. Although studies have identified genes and pathways frequently mutated in B-cell lymphoma[3-8], many tumors have no detectable driver mutations and we do not yet have complete understanding of the genetic alterations necessary for tumor development[6].

The search for driver mutations in B-cell lymphoma has however been primarily restricted to coding regions[3-6]. Gene regulation is highly cell-type specific, and the interpretation of mutations within non-coding regions of lymphoma genomes has been in part constrained by a lack of information on relevant regulatory elements and their target genes[9,10]. Furthermore, although mutation recurrence is an indicator of positive selection in tumors, the sheer size of the non-coding genome places a high statistical burden on an ability to distinguish passenger from driver mutations.

Cis-regulatory elements (CREs) and promoters controlling gene expression represent a highly enriched subset of the non-coding genome in which to search for potential driver mutations[11]. Herein we have exploited this principle by using information from promoter

capture Hi-C (CHi-C) in naïve B cells[12] in an analysis of whole-genome sequencing (WGS) data on 80 DLBCL and 37 FL tumors. By linking CRE mutation to gene expression (**Figure 1**), we identify recurrently mutated non-coding regulatory regions, enhancing our understanding of the oncogenic pathways and mechanisms relevant to B-cell lymphoma biology.

METHODS

Sequencing data

Data from 40 DLBCL, 37 FL and 61 chronic lymphocytic leukemia (CLL) tumors, and matched normal samples, were obtained from the International Cancer Genome Consortium (ICGC)[5,13]. Data from an additional 40 DLBCL tumors and matched normal samples were obtained from The Cancer Genome Characterization Initiative (CGCI)[8]. The ICGC data has been aligned, processed and variants called as part of the Pan-Cancer Analysis of Whole Genomes (PCAWG) project. A consensus approach to variant calling was adopted by PCAWG, combining the results of multiple pipelines to call SNVs, indels, CNVs and SVs (https://github.com/ICGC-TCGA-PanCancer). For each mutation type we downloaded and used variants called by a respective pipeline. To minimize technical differences between the cohorts, we aligned, processed and called variants in the CGCI data using identical pipelines, as described in Supplementary Methods. RNA-sequencing data for all samples were obtained from the CGCI and ICGC and processed as described in Supplementary Methods. This study uses only published sequencing data and therefore ethical approval was not sought.

Definition of regulatory regions

Promoter regions were defined as the intervals spanning 400bp upstream to 250bp downstream of transcription start sites from RefGene[14]. CREs were defined using promoter CHi-C data generated on naïve B cells[12]. HindIII fragments interacting with at least one protein-coding gene promoter were considered CREs. Only promoter-CRE interactions with a CHiCAGO score ≥5[15] and a linear distance ≤5Mb[16] were included in the analysis. Additional

filtering the CHi-C data was completed to reduce false identification of interactions (**Supplementary Methods**).

Analysis of recurrent mutation of regulatory regions

Promoters and CREs were tested independently for recurrent mutation across tumors above that expected given the background mutation rates, using a Poisson binomial model as *per* Melton *et al.*[17]. We employed a Poisson binomial model as it allowed us to consider tumor-specific mutation rates[17], which is not possible using many alternative approaches[18,19]. Briefly, the mutation probability of each regulatory region in each tumor was computed by fitting a logistic regression model to all data, taking into account the following features: tumor ID, mutation trinucleotide context, regional replication timing and 1Mb mutational density. Replication timing was estimated as the mean of replication timing data from HeLa, HepG2, K562, MCF-7 and SK-N-SH cell lines[20]. Promoters and CREs overlapping open reading frames (defined in Ensembl v73), extended 5bp in each direction to account for splice sites, were excluded from the analysis[18] Regions of CREs overlapping 3' UTR and 5' UTR were also excluded from the analysis[18].

The probability that a region is mutated was defined as:

$$P(\text{region is mutated}) = 1 - \prod_{i=1}^{s}(1 - p_i)$$

where *i* is the base position, *s* is the number of nucleotides considered in the region (*i.e.* not excluded) and p_i is the probability that a mutation occurs at base *i. P*-values were computed for each promoter and CRE using an approximation of the Poisson binomial model implemented in the poibin R-package[17]. Recurrent mutation *P*-values follow a discreet

distribution and we therefore used the right tail masses to compute randomized *P*-values for each region[21].

Relationship between simple somatic mutations at CREs and gene expression

Significantly mutated CREs were examined for differential expression of target genes between mutated and non-mutated tumors. For each CRE, tumors were classified mutated or non-mutated based on the presence of SNVs or indels at the CRE, and differential expression assessed using permutation testing[22]. In the permutation testing a *t*-test was performed using the mutated/non-mutated tumor labels to generate a single *t*-value (the observed *t*-value). The expression values for the mutated/non-mutated tumors were then permuted 10,000 times to generate 10,000 additional *t*-values (the permutated *t*-values). The permuted *t*-values generally fit a Gaussian distribution, against which the observed *t*-value could be compared using a two-tailed test[22]. Samples with CNVs at either the CRE or target gene were excluded. Additionally, samples with translocation or inversion breakpoints ≤1Mb from the target gene were excluded. Only CREs mutated in at least five tumors were tested, after removal of tumors with CNVs at the CRE or target gene, or proximal translocation or inversion breakpoints. CREs interacting with multiple gene promoters were tested multiple times. Only CREs interacting with the promoters of protein-coding genes were examined. The Benjamini-Hochberg procedure was used to adjust for multiple testing and significance thresholded at $Q<0.1$.

Relationship between CNVs at CREs and gene expression

Focal amplifications and deletions were defined as absolute copy number changes ≥1 and size ≤3Mb. To identify tumors with CNVs at CREs driving altered gene expression we (i)

identified tumors with amplifications or deletions at a CRE, (ii) excluded tumors with CNVs at the target gene, (iii) excluded tumors with translocation or inversion breakpoints ≤1Mb from the target gene, and (iv) assessed the association between the copy number change *d* and $\log_2$-transformed gene expression *e* by fitting a linear regression model: $e = \beta_0 + \beta_1 d$. A *t*-statistic was computed using the estimated β_1 coefficient and standard error, and a *P*-value was computed from this *t*-statistic under the null hypothesis of no association between copy number change and gene expression ($\beta_1 = 0$). Only regulatory regions mutated in at least five tumors were tested, after exclusion of tumors with CNVs at the target gene or proximal translocation and inversion breakpoints. Copy number changes were calculated relative to the ploidy of the tumor, as determined by ascatNgs[23]. For simplicity, all losses and gains were considered equally when calculating correlation coefficients (*i.e.* each tumor is defined as having either a loss, no change, or gain in copy number). In addition to conducting individual analyses of DLBCL and FL tumors, we completed a meta-analysis of the two tumor types under a fixed effects model. The Benjamini-Hochberg procedure was used to adjust for multiple testing and significance thresholded at *Q*<0.1.

Survival analysis

To examine the relationship between gene expression and overall survival, we made use of data from three independent DLBCL patient cohorts from Barrans *et al.*[24], Lenz *et al*.[25] and Reddy *et al*.[6], which were downloaded from GEO. Patients were censored based on their last known clinical follow up. For each series, gene expression was first treated as a continuous variable in a Cox proportional hazards model with inclusion of age at diagnosis, sex, COO and treatment received (chemotherapy or rituximab-chemotherapy) as covariates.

Analysis was performed using the log-rank test to estimate expression-associated HRs, and the Wald test was used to determine statistical significance. The proportional hazards assumption in the Cox models was assessed using scaled Schoenfeld residuals implemented in the "cox.zph" function from the survival R-package. Meta-analyses of the independent patient cohorts were performed under a fixed-effects model. We also stratified cancers by the expression of the gene, defining tumors as having high or low expression of a gene if the expression value was within the top or bottom third of expression values for the gene across all cancers respectively. Kaplan-Meier analysis was then performed using this tumor stratification and the difference between the survival distributions assessed using the log-rank test.

Data availability

ICGC data, processed as part of the PCAWG project, were downloaded from the ICGC Data Coordination Center (DCC) Data Portal (project codes MALY-DE and CLLE-ES). CGCI data were downloaded from dbGaP (phs000532.v7). Naïve B-cell CHi-C data were obtained from Javierre *et al*[12]. Histone ChIP-seq data were downloaded from BLUEPRINT (sample C005Q). Clinical and gene expression data used in survival analyses were downloaded from GEO (GSE32918 and GSE10846) and obtained from Reddy *et al*[6].

RESULTS

Recurrently mutated non-coding regulatory regions

After quality control and filtering of WGS data, we identified 1,169,005 single nucleotide variants (SNVs) in the DLBCL tumors (5.07 mutations per megabase [Mb]), and 255,889 SNVs in FL tumors (2.40 mutations per Mb; **Table S1**). Recurrently mutated regions were identified as those containing a greater number of mutations than that expected given the background mutation rate, adjusting for tumor-specific mutation rates, trinucleotide contexts, replication timing and 1Mb mutational density[17]. To identify somatic mutations in non-coding regulatory regions, we defined 21,750 regions associated with 17,677 genes as promoters[14]. We identified recurrently mutated promoters associated with 17 and 4 genes in DLBCL and FL tumors respectively (Q<0.1, **Table S2**). These genes include *BLK, IRF8* and *SPIB*, which are implicated in lymphoma development and growth[26-28], but for which recurrent promoter mutations have not previously been reported[9].

Using promoter CHi-C in naïve B cells[12] we defined 69,872 genomic fragments containing putative CREs (median size 2.1Kb), involved in 142,791 unique significant interactions with promoters (median linear distance 292Kb) and constituting 7% of the genome. These promoter-interacting fragments have previously been shown to be enriched for ATAC-seq accessibility and regulatory histone marks[12]. We identified 78 recurrently mutated CREs interacting with the promoters of 72 genes in DLBCL tumors (Q<0.1, **Table S3**), and 42 recurrently mutated CREs interacting with the promoters of 37 genes in FL tumors (Q<0.1, **Table S3**). The majority of these recurrently mutated CREs (59% in DLBCL and 63% in FL) do not interact with the promoter of the closest gene, but with the promoters of more distal

genes. Genes targeted by recurrently mutated CREs include *PAX5*, which interacts with ten and eight recurrently mutated CRE fragments in DLBCL and FL respectively, and whose expression is disrupted by non-coding mutations in chronic lymphoblastic leukemia (CLL)[13] and multiple myeloma (MM)[29]. Furthermore, we identified recurrently mutated CREs interacting with genes known to also be affected by coding mutations, including five genes previously associated with non-coding mutations in B-cell lymphoma (*ARID5B*, *BCL2*, *BCL6*, *ETS1*, *PAX5*) and five genes for which only coding mutations have previously been reported (*DMXL1*, *IKZF3*, *PCDHB1*, *SEMA3D* and *SYPL1;* **Table S3**)[6,7,9,10].

We used Palimpsest to characterise the processes most likely to be responsible for the recurrent mutation of promoters and CREs (**Tables S4, S5** and **S6**; **Supplementary Methods**)[30-32]. In DLBCL, promoters and CREs of genes including *BCL6* were enriched for mutations attributed to signatures SBS84 or SBS85 ($P < 0.05$; **Table S4**), which are associated with the activity of activation-induced deaminase (AID)[32], supporting previous observations[33]. Furthermore, the promoters and CREs of multiple genes, including *SGK1* and *ST6GAL1* in DLBCL, were enriched for mutations attributed to signature SBS3 (**Table S4** and **S5**), which is indicative of defective homologous recombination repair[34], consistent with distinct processes underling the mutation of different regulatory elements.

To identify non-coding driver mutations in regulatory regions, we compared the expression levels of target genes of recurrently mutated CREs between mutated and non-mutated tumors, using RNAseq data from each tumor. Tumors with copy number changes overlapping either the CRE or target gene, and tumors with translocation or inversion breakpoints ≤1Mb from the target gene were excluded from this analysis. Mutation of a CRE

interacting with the *TPRG1* promoter, occurring in nine tumors (**Figure 2**), was associated with increased *TPRG1* expression in DLBCL (*Q*=0.09, **Figure 3**, **Table S7**). This CRE is annotated by epigenetic marks indicative of active enhancers (**Figure 3, Figure S1, Supplementary Methods**) and located at a regulatory region previously identified in DLBCL to be bound by the bromodomain 4 (BRD4) chromatin reader protein (**Figure 3A, Supplementary Methods**)[35], which is characteristic of enhancers important in DLBCL growth and cell cycle progression[35]. Amplifications of the *TPRG1* gene were present in an additional 18 DLBCL tumors, with the mutation of recurrently mutated *TPRG1* CREs and *TPRG1* gene amplifications tending to occur in different tumors (*P*=0.016, two-tailed Fisher's exact test), suggesting alternative mechanisms of gene dysregulation. Whilst the mutation of this region has previously been reported in B-cell lymphoma, it was not previously associated with disrupted *TPRG1* expression[9]. This *TPRG1* CRE is enriched for mutations attributed to signatures SBS84 *(P*=0.002) and SBS85 (*P*=0.030) (**Table S5**), consistent with it being a target of AID activity[32,36]. Whilst the function of *TPRG1* is poorly characterized, it is regulated by p63[37], which has been implicated as playing a role in lymphoma oncogenesis[38].

Copy number variation at CREs dysregulates gene expression

To identify CREs subject to somatic copy number variation (CNV), we identified CNVs in tumors using WGS data (**Figure 2**). CNV-positive CREs were assessed for a correlation with the expression of target genes, excluding cases where the gene was encompassed by a CNV, using RNAseq data from each tumor. In DLBCL tumors, 20 CNV-positive CREs were associated with target gene expression (*Q*<0.1, **Table S8**), 19 of which are located in a 220Kb region on chromosome 14. In FL tumors, two CNV-positive CREs, located in the same region of chromosome 14, were associated with target gene expression (*Q*<0.1, **Table S8**).

The *CD69* promoter interacts with a CRE annotated by multiple epigenetic marks, overlapping a DLBCL BRD4-bound regulatory region (**Figure 4A**, **Figure S2**)[35]. This CRE region is deleted in five DLBCL tumors, which were associated with higher *CD69* expression (*Q*=0.06, **Figure 4B, Table S8**), suggesting this element acts as a repressor of *CD69* expression. *CD69* plays a role in B-cell development in mice[39] and enhanced antitumor immunity has been observed in mice deficient in *CD69*[40]. Higher *CD69* protein expression has previously been associated with shorter survival in B-cell lymphoma patients[41,42], although we did not replicate this association with RNA expression in three independent series totaling 1,670 DLBCL cases (**Table S9**). Whilst deletion of the *CD69* CRE was accompanied by *ETV6* exon deletions in three of the five tumors, altered *ETV6* expression was not observed in these samples (**Figure 4C**)**.**

The T-cell receptor alpha (TRA) locus, which undergoes V(D)J recombination during T-cell development[43], is the subject of copy number losses and gains in both DLBCL and FL tumors (**Table S8**). This region is annotated with multiple histone marks and contains two DLBCL BRD4-bound regulatory regions[35] (**Figure 5A, Figure S3**). In DLBCL, eight CRE fragments at the *TRA* locus were deleted in 20 and amplified in 11 tumors. These CRE fragments contact the promoters of 16 genes, with copy number changes associated with the expression of *ABHD4, LRP10*, *MMP14*, *PRMT5* and *SLC7A7* (*Q*<0.1, **Figure 5B**-**C**, **Table S8**). In FL, these CRE fragments were deleted in 17 tumors and amplified in one, with copy number changes associated with the expression of only *ACIN1* (*Q*=0.04, **Table S8**). In the DLBCL tumors, increased CRE copy number was associated with reduced *MMP14* expression (*Q*=0.03, **Figure 5B**). *MMP14* is well established to negatively regulate Notch signaling[44], a pathway

disrupted in DLBCL[45], and through which the loss of *MMP14* impairs B-cell differentiation[44]. Lower *MMP14* expression was associated with worse overall survival in DLBCL (hazard ratio [HR]=0.85, 95% confidence interval [CI]: 0.77-0.95, *P*=0.003, **Figure S4**, **Table S9**). Increased CRE copy number was associated with increased *PRMT5* expression in DLBCL tumors (*Q*=0.03), although this trend in expression was driven by lower *PRMT5* expression in tumors with CRE deletions, as increased *PRMT5* expression was not observed in tumors with CRE amplifications (**Figure 5C**).

Although copy number changes at the TRA locus have previously been observed in B-cell malignancies[46-48], it is disputed whether these variants are pathogenic lesions occurring in the tumor cells[46], or whether they occur not in the tumor cells but in infiltrating T-cells[47], which are often found in lymphoma as part of the immune response[49]. To assess whether infiltrating T cells may be responsible for CNVs at the TRA locus, we addressed the potential issue of normal contamination using tumor purity estimates from ascatNgs for each sample. CNV calling by ascatNgs is suboptimal where there is >50% contamination[50]. In view of this, T-cell contamination is less likely to be responsible for observed CNVs when normal contamination is <50%. In 15/20 of DLBCL samples and 11/17 of FL samples with TRA locus deletions, normal contamination was >50%, suggesting that the TRA locus losses observed in these samples may not occur in cancer cells, but instead in infiltrating T-cells. Conversely, in all 11 DLBCL samples and in the one FL sample with TRA locus amplifications, normal contamination was <50%, consistent with TRA locus amplification being more likely associated with tumor cells, rather than infiltrating cells.

Many CREs are affected by expression-associated CNVs in both DLBCL and FL tumors (**Table S8**) and we therefore conducted a meta-analysis of these association statistics under a fixed-effects model (**Table S10**). In this meta-analysis, CNV-positive CREs interacting with the promoters of *MMP14, PRMT5* and *SLC7A7* were associated with the expression of these genes (Q<0.1), suggesting a common effect of these CNVs on target gene expression in these B-cell malignancies.

Meta-analysis of the DLBCL and FL tumors also identified two CREs interacting with the *IGLL5* promoter, for which focal deletion was associated with lower *IGLL5* expression (Q<0.1, **Table S10**). The CNV-positive CRE most strongly association with *IGLL5* expression (Q=0.03, **Figure 6A-D**) was deleted in 14 DLBCL tumors and 6 FL tumors, and annotated by epigenetic marks indicative of active enhancers (**Figure 6A**, **Figure S5**). Whilst the function of *IGLL5* remains to be established, it is recurrently mutated in DLBCL[51], and is homologous to *IGLL1*, a gene which plays a critical role in B-cell development[52]. Furthermore, *IGLL5* has been shown to function as a tumor suppressor in a CRISPR-based screen of DLBCL cell lines[6], a finding in keeping with reduced *IGLL5* expression being associated with CRE deletion. Although focal deletion of regions encompassing the *IGLL5* CRE occur in other B-cell malignancies, including childhood acute lymphoblastic leukemia (ALL)[53] and CLL[54], their pathogenicity is unclear[54,55]. Since the *IGLL5* CRE is located at the immunoglobulin lambda light chain locus (IGL) Mraz *et al.* postulated that such deletions are likely to merely be the consequence of IGL rearrangements[55]. Conversely, Mangum *et al.* has shown that the locus deletions observed in ALL occur independently of IGL rearrangement and frequently do not involve the VJ junction nor follow the ordered model of V(D)J recombination[53]. Many of the CNVs observed in the DLBCL and FL tumors similarly do not involve the VJ junction (**Figure**

6A), suggesting that they also occur independently of V(D)J recombination. As focal deletion of this region has previously been observed in CLL[54], we completed a secondary analysis of this CRE in 61 CLL tumors[13]. In these tumors deletion of the CRE was also associated with lower *IGLL5* expression (P=6.1×10^{-7}, **Figure 6D**), suggesting that the effect of the deletion of this CRE on *IGLL5* expression may be generic to B-cell malignancies.

We examined whether tumors harboring CNV-positive CREs associated with target gene expression were enriched for DLBCL tumors of either the activated B-cell-like (ABC) or germinal center B-cell-like (GCB) cell-of-origin (COO) subtypes (**Table S11, Supplementary Methods**). Although *CD69* CRE deletions were observed exclusively in ABC or unclassified tumors, this enrichment was non-significant (P=0.16).

Pathways targeted by both coding and non-coding mutation in DLBCL

To better inform the interplay between non-coding driver mutations with other driver mechanisms, we identified pathways targeted by coding and non-coding mutations, combining genes identified in this analysis and genes with recurrent coding mutations from an analysis of 1,001 DLBCL whole exomes[6] (**Table S12**, **Supplementary Methods**). One pathway identified is Notch signaling (Q=2.1×10^{-4}), which contains genes affected by coding mutations, such as *CREBBP*, and genes affected by non-coding mutations, such as *IKZF1* and *PLXND1*. Other pathways affected by both coding and non-coding mutations include DNA repair, transcriptional regulation by TP53, and WNT-signaling (Q<0.1), all of which are linked to B-cell lymphoma development[56].

DISCUSSION

This analysis has identified putative non-coding driver mutations in B-cell lymphoma and highlights that pathways key to lymphomagenesis can be targeted somatically through multiple mechanisms. Using promoter CHi-C, we identify recurrently mutated CREs and link them to the genes they regulate. By adopting this strategy we have sought to address the issue that many recurrently mutated CREs will not necessarily interact with the promoter of the proximal gene and hence the target gene will remain unidentified. This is illustrated by the CREs interacting with the promoters of *IGLL5* and *TPRG1*, neither of which interact with their proximal genes, but whose mutation is associated with dysregulated expression of the respective target gene.

It has previously been demonstrated that disruption of the Notch-signaling pathway, through coding mutations in genes such as *NOTCH2* and *FBXW7,* confers an unfavorable prognosis in DLBCL[57]. Here we add *MMP14* to the list of genes in this pathway disrupted in DLBCL, the lower expression of which is similarly associated with worse survival (**Table S9**).

V(D)J recombinase recognizes recombination sequence signals (RSSs), which consist of conserved heptamer and nonamer elements separated by a spacer[58]. We identified RSS sites adjacent to the boundaries of 11/49 TRA locus CNVs, 10/25 *IGLL5* CRE CNVs, and 0/5 *CD69* CRE CNVs (**Table S13**). Calling RSS sites is inherently difficult, due to some sites being less conserved nor adjacent to identified breakpoints[59]. Therefore, whilst this analysis provides no evidence that many of the CRE-disrupting CNVs occur due to V(D)J recombination, we cannot exclude this possibility.

Here we utilize naïve B-cell CHi-C data to characterize CREs and map them to their respective target genes. DLBCL and FL tumors develop from B cells at various stages of differentiation[1], and naïve B-cell CHi-C data may therefore not fully recapitulate the regulatory interactions active in each tumors' COO. Nevertheless, many interactions involving mutated CREs associated with differential target gene expression are also observed in total B-cell CHi-C data (**Table S14**)[12], suggesting that these interactions may not be unique to a single stage of B-cell differentiation. These CREs are also annotated by epigenetic marks indicative of active enhancers in B cells at different differentiation stages (**Figures S1-S3** and **S5**), indicating that the activity of these CREs is not restricted to a single differentiation stage.

We acknowledge that this analysis has limitations. Firstly, when evaluating the effect of CRE mutations on gene expression we consider all CRE mutations to be potential drivers. It is also possible that some CREs contain a mixture of mutations that do and do not affect gene expression, thereby reducing study power. Secondly, we do not consider the clonality of mutations in the differential expression analysis. Thirdly, we did not assess whether CRE mutations affect promoter interactions or the affinity of transcription factors. CRISPR/Cas9-based genome editing and electrophoretic mobility shift assays could be used to investigate the functional impact of these mutations.

In summary, our findings highlight the contribution of non-coding mutations and CNVs to B-cell lymphomagenesis, and provide further insight into the genetic complexity of B-cell lymphoma. Furthermore this study illustrates the advantages of using information from

chromosome conformation capture to decode regulatory elements relevant to B-cell lymphoma.

ACKNOWLEDGEMENTS

This work is funded by grants from Bloodwise and Cancer Research UK. The results published here are part based upon data generated by the CGCI, Non-Hodgkin Lymphoma project, developed and managed by the NCI. Information about CGCI projects can be found at https://ocg.cancer.gov/programs/cgci. This study makes use of data from ICGC, processed as part of the PCAWG project. We would like to thank the clinical contributors and data producers for these projects. This study also makes use of data generated by the Blueprint Consortium. A full list of the investigators who contributed to the generation of the data is available from www.blueprint-epigenome.eu. Funding for the project was provided by the European Union's Seventh Framework Programme (FP7/2007-2013) under grant agreement no 282510 BLUEPRINT.

AUTHORSHIP CONTRIBUTIONS

A.J.C. and R.S.H. conceived and designed the study. A.J.C., P.H.H., S.E.D., P.J.L., D.C. and G.O. performed bioinformatic analyses. A.J.C. performed statistical analyses. A.J.C. and R.S.H. wrote the manuscript, with contributions from P.H.H., D.C. and G.O. All authors reviewed the final manuscript.

DISCLOSURE OF CONFLICTS OF INTEREST

The authors declare no conflict of interest.

REFERENCES

1. Campo E, Swerdlow SH, Harris NL, Pileri S, Stein H, Jaffe ES. The 2008 WHO classification of lymphoid neoplasms and beyond: evolving concepts and practical applications. *Blood*. 2011;117(19):5019-5032.

2. Smith A, Crouch S, Lax S, et al. Lymphoma incidence, survival and prevalence 2004-2014: sub-type analyses from the UK's Haematological Malignancy Research Network. *Br J Cancer*. 2015;112(9):1575-1584.

3. Pasqualucci L, Dominguez-Sola D, Chiarenza A, et al. Inactivating mutations of acetyltransferase genes in B-cell lymphoma. *Nature*. 2011;471(7337):189-195.

4. Lohr JG, Stojanov P, Lawrence MS, et al. Discovery and prioritization of somatic mutations in diffuse large B-cell lymphoma (DLBCL) by whole-exome sequencing. *Proc Natl Acad Sci U S A*. 2012;109(10):3879-3884.

5. Richter J, Schlesner M, Hoffmann S, et al. Recurrent mutation of the ID3 gene in Burkitt lymphoma identified by integrated genome, exome and transcriptome sequencing. *Nat Genet*. 2012;44(12):1316-1320.

6. Reddy A, Zhang J, Davis NS, et al. Genetic and Functional Drivers of Diffuse Large B Cell Lymphoma. *Cell*. 2017;171(2):481-494 e415.

7. Zhang J, Grubor V, Love CL, et al. Genetic heterogeneity of diffuse large B-cell lymphoma. *Proc Natl Acad Sci U S A*. 2013;110(4):1398-1403.

8. Morin RD, Johnson NA, Severson TM, et al. Somatic mutations altering EZH2 (Tyr641) in follicular and diffuse large B-cell lymphomas of germinal-center origin. *Nat Genet*. 2010;42(2):181-185.

9. Mathelier A, Lefebvre C, Zhang AW, et al. Cis-regulatory somatic mutations and gene-expression alteration in B-cell lymphomas. *Genome Biol*. 2015;16:84.

10. Arthur SE, Jiang A, Grande BM, et al. Genome-wide discovery of somatic regulatory variants in diffuse large B-cell lymphoma. *Nat Commun*. 2018;9(1):4001.

11. Orlando G, Law PJ, Cornish AJ, et al. Promoter capture Hi-C-based identification of recurrent noncoding mutations in colorectal cancer. *Nat Genet*. 2018;50(10):1375-1380.

12. Javierre BM, Burren OS, Wilder SP, et al. Lineage-Specific Genome Architecture Links Enhancers and Non-coding Disease Variants to Target Gene Promoters. *Cell*. 2016;167(5):1369-1384 e1319.

13. Puente XS, Bea S, Valdes-Mas R, et al. Non-coding recurrent mutations in chronic lymphocytic leukaemia. *Nature*. 2015;526(7574):519-524.

14. Rheinbay E, Parasuraman P, Grimsby J, et al. Recurrent and functional regulatory mutations in breast cancer. *Nature*. 2017;547(7661):55-60.

15. Cairns J, Freire-Pritchett P, Wingett SW, et al. CHiCAGO: robust detection of DNA looping interactions in Capture Hi-C data. *Genome Biol*. 2016;17(1):127.

16. Dryden NH, Broome LR, Dudbridge F, et al. Unbiased analysis of potential targets of breast cancer susceptibility loci by Capture Hi-C. *Genome Res*. 2014;24(11):1854-1868.

17. Melton C, Reuter JA, Spacek DV, Snyder M. Recurrent somatic mutations in regulatory regions of human cancer genomes. *Nat Genet*. 2015;47(7):710-716.

18. Weinhold N, Jacobsen A, Schultz N, Sander C, Lee W. Genome-wide analysis of noncoding regulatory mutations in cancer. *Nat Genet*. 2014;46(11):1160-1165.

19. Nik-Zainal S, Davies H, Staaf J, et al. Landscape of somatic mutations in 560 breast cancer whole-genome sequences. *Nature*. 2016;534:47-54.

20. Hansen RS, Thomas S, Sandstrom R, et al. Sequencing newly replicated DNA reveals widespread plasticity in human replication timing. *Proc Natl Acad Sci U S A*. 2010;107(1):139-144.

21. Imielinski M, Guo G, Meyerson M. Insertions and Deletions Target Lineage-Defining Genes in Human Cancers. *Cell*. 2017;168(3):460-472 e414.

22. Feigin ME, Garvin T, Bailey P, et al. Recurrent noncoding regulatory mutations in pancreatic ductal adenocarcinoma. *Nat Genet*. 2017;49(6):825-833.

23. Raine KM, Van Loo P, Wedge DC, et al. ascatNgs: Identifying Somatically Acquired Copy-Number Alterations from Whole-Genome Sequencing Data. *Curr Protoc Bioinformatics*. 2016;56:15 19 11-15 19 17.

24. Barrans SL, Crouch S, Care MA, et al. Whole genome expression profiling based on paraffin embedded tissue can be used to classify diffuse large B-cell lymphoma and predict clinical outcome. *Br J Haematol*. 2012;159(4):441-453.

25. Lenz G, Wright G, Dave SS, et al. Stromal gene signatures in large-B-cell lymphomas. *N Engl J Med*. 2008;359(22):2313-2323.

26. Xu Y, Jiang L, Fang J, et al. Loss of IRF8 Inhibits the Growth of Diffuse Large B-cell Lymphoma. *J Cancer*. 2015;6(10):953-961.

27. Petersen DL, Berthelsen J, Willerslev-Olsen A, et al. A novel BLK-induced tumor model. *Tumour Biol*. 2017;39(7):1010428317714196.

28. Takagi Y, Shimada K, Shimada S, et al. SPIB is a novel prognostic factor in diffuse large B-cell lymphoma that mediates apoptosis via the PI3K-AKT pathway. *Cancer Sci*. 2016;107(9):1270-1280.

29. Hoang PH, Dobbins SE, Cornish AJ, et al. Whole-genome sequencing of multiple myeloma reveals oncogenic pathways are targeted somatically through multiple mechanisms. *Leukemia*. 2018.

30. Shinde J, Bayard Q, Imbeaud S, et al. Palimpsest: an R package for studying mutational and structural variant signatures along clonal evolution in cancer. *Bioinformatics*. 2018;34(19):3380-3381.

31. Letouze E, Shinde J, Renault V, et al. Mutational signatures reveal the dynamic interplay of risk factors and cellular processes during liver tumorigenesis. *Nat Commun*. 2017;8(1):1315.

32. Alexandrov L, Kim J, Haradhvala NJ, et al. The Repertoire of Mutational Signatures in Human Cancer. *bioRxiv*. 2018.

33. Alvarez-Prado AF, Perez-Duran P, Perez-Garcia A, et al. A broad atlas of somatic hypermutation allows prediction of activation-induced deaminase targets. *J Exp Med*. 2018;215(3):761-771.

34. Alexandrov LB, Nik-Zainal S, Wedge DC, et al. Signatures of mutational processes in human cancer. *Nature*. 2013;500(7463):415-421.

35. Chapuy B, McKeown MR, Lin CY, et al. Discovery and characterization of super-enhancer-associated dependencies in diffuse large B cell lymphoma. *Cancer Cell*. 2013;24(6):777-790.

36. Kasar S, Kim J, Improgo R, et al. Whole-genome sequencing reveals activation-induced cytidine deaminase signatures during indolent chronic lymphocytic leukaemia evolution. *Nat Commun*. 2015;6:8866.

37. Antonini D, Dentice M, Mahtani P, et al. Tprg, a gene predominantly expressed in skin, is a direct target of the transcription factor p63. *J Invest Dermatol*. 2008;128(7):1676-1685.

38. Fukushima N, Satoh T, Sueoka N, et al. Clinico-pathological characteristics of p63 expression in B-cell lymphoma. *Cancer Sci*. 2006;97(10):1050-1055.

39. Lauzurica P, Sancho D, Torres M, et al. Phenotypic and functional characteristics of hematopoietic cell lineages in CD69-deficient mice. *Blood*. 2000;95(7):2312-2320.

40. Esplugues E, Sancho D, Vega-Ramos J, et al. Enhanced antitumor immunity in mice deficient in CD69. *J Exp Med*. 2003;197(9):1093-1106.

41. Erlanson M, Gronlund E, Lofvenberg E, Roos G, Lindh J. Expression of activation markers CD23 and CD69 in B-cell non-Hodgkin's lymphoma. *Eur J Haematol*. 1998;60(2):125-132.

42. Del Poeta G, Del Principe MI, Zucchetto A, et al. CD69 is independently prognostic in chronic lymphocytic leukemia: a comprehensive clinical and biological profiling study. *Haematologica*. 2012;97(2):279-287.

43. Livak F, Schatz DG. T-cell receptor alpha locus V(D)J recombination by-products are abundant in thymocytes and mature T cells. *Mol Cell Biol*. 1996;16(2):609-618.

44. Jin G, Zhang F, Chan KM, et al. MT1-MMP cleaves Dll1 to negatively regulate Notch signalling to maintain normal B-cell development. *EMBO J*. 2011;30(11):2281-2293.

45. Lee SY, Kumano K, Nakazaki K, et al. Gain-of-function mutations and copy number increases of Notch2 in diffuse large B-cell lymphoma. *Cancer Sci*. 2009;100(5):920-926.

46. Nacheva EP, Brazma D, Virgili A, et al. Deletions of immunoglobulin heavy chain and T cell receptor gene regions are uniquely associated with lymphoid blast transformation of chronic myeloid leukemia. *BMC Genomics*. 2010;11:41.

47. Broseus J, Chen G, Hergalant S, et al. Relapsed diffuse large B-cell lymphoma present different genomic profiles between early and late relapses. *Oncotarget*. 2016;7(51):83987-84002.

48. Bignell GR, Greenman CD, Davies H, et al. Signatures of mutation and selection in the cancer genome. *Nature*. 2010;463(7283):893-898.

49. Keane C, Gould C, Jones K, et al. The T-cell Receptor Repertoire Influences the Tumor Microenvironment and Is Associated with Survival in Aggressive B-cell Lymphoma. *Clin Cancer Res*. 2017;23(7):1820-1828.

50. Chen GK, Chang X, Curtis C, Wang K. Precise inference of copy number alterations in tumor samples from SNP arrays. *Bioinformatics*. 2013;29(23):2964-2970.

51. de Miranda NF, Georgiou K, Chen L, et al. Exome sequencing reveals novel mutation targets in diffuse large B-cell lymphomas derived from Chinese patients. *Blood*. 2014;124(16):2544-2553.

52. Thompson EC, Cobb BS, Sabbattini P, et al. Ikaros DNA-binding proteins as integral components of B cell developmental-stage-specific regulatory circuits. *Immunity*. 2007;26(3):335-344.

53. Mangum DS, Downie J, Mason CC, et al. VPREB1 deletions occur independent of lambda light chain rearrangement in childhood acute lymphoblastic leukemia. *Leukemia*. 2014;28(1):216-220.

54. Gunn SR, Bolla AR, Barron LL, et al. Array CGH analysis of chronic lymphocytic leukemia reveals frequent cryptic monoallelic and biallelic deletions of chromosome 22q11 that include the PRAME gene. *Leuk Res*. 2009;33(9):1276-1281.

55. Mraz M, Stano Kozubik K, Plevova K, et al. The origin of deletion 22q11 in chronic lymphocytic leukemia is related to the rearrangement of immunoglobulin lambda light chain locus. *Leuk Res*. 2013;37(7):802-808.

56. Basso K, Dalla-Favera R. Germinal centres and B cell lymphomagenesis. *Nat Rev Immunol*. 2015;15(3):172-184.

57. Karube K, Martinez D, Royo C, et al. Recurrent mutations of NOTCH genes in follicular lymphoma identify a distinctive subset of tumours. *J Pathol*. 2014;234(3):423-430.

58. Hesse JE, Lieber MR, K. M, Gellert M. V(D)J recombination: a functional definition of the joining signals. *Genes and Development*. 1989;3(7):1053-1061.

59. Papaemmanuil E, Rapado I, Li Y, et al. RAG-mediated recombination is the predominant driver of oncogenic rearrangement in ETV6-RUNX1 acute lymphoblastic leukemia. *Nature Genetics*. 2014;42(2):116-125.

60. Skidmore ZL, Wagner AH, Lesurf R, et al. GenVisR: Genomic Visualizations in R. *Bioinformatics*. 2016;32(19):3012-3014.

FIGURE LEGENDS

Figure 1: Analysis overview. CGCI: The Cancer Genome Characterization Initiative, ICGC: The International Cancer Genome Consortium, DLBCL: diffuse large B-cell lymphoma, FL: follicular lymphoma, SNV: single nucleotide variant, CNV: copy number variant, CRE: *cis*-regulatory element, CHi-C: capture Hi-C.

Figure 2: Overview of CRE mutations, amplifications and losses associated with altered target gene expression in DLBCL and FL. Top panel shows the genome-wide mutation burden for each tumor. Second panel shows the occurrence of SNVs in the *TPRG1* CRE. Third panel shows the occurrence of amplifications and losses at CREs associated with altered target gene expression. Bottom panel indicates the disease type and the cell of origin of each tumor. Figure generated using GenVisR[60].

Figure 3: Single nucleotide variants at *cis*-regulatory element are associated with *TPRG1* expression in DLBCL. (A) SNVs at a CRE interacting with the *TPRG1* promoter. Top panel shows position of SNVs at the CRE. Second panel shows chromatin looping interactions between the *TPRG1* promoter and CREs, with the interaction between the promoter and the SNV-disrupted CRE colored yellow. Third panel details ChIP-seq histone mark signals in naïve B-cells. Bottom panels show positions of BRD4-bound enhancers in DLBCL[35]. (B) CRE mutation status and gene expression. Whilst the *TPRG1* CRE is mutated in nine DLBCL tumors, only six tumors are considered in the differential expression analysis, as three tumors have CNVs at the CRE or target gene. Differential expression assessed using *t*-value

permutation test. Boxplot hinges extend to the most extreme data points that are no more than 1.5 times the interquartile range from the box.

Figure 4: Copy number variation at *cis*-regulatory element is associated with *CD69* expression in DLBCL. (A) Loss of a CRE interacting with the *CD69* promoter. Top panel shows position of CNVs at CRE, all of which are copy number losses. Second panel shows chromatin looping interactions between the *CD69* promoter and CREs, with the interaction between the promoter and the CNV-disrupted CRE colored yellow. Third panel details ChIP-seq histone mark signals in naïve B-cells. Bottom panel shows positions of BRD4-bound enhancers in DLBCL[35]. (B) CNV status at CRE and *CD69* expression in DLBCL tumors. (C) CNV status at CRE and *ETV6* expression in DLBCL tumors. Association between copy number status and gene expression assessed through linear regression. Boxplot hinges extend to the most extreme data points that are no more than 1.5 times the interquartile range from the box.

Figure 5: Copy number variation at *cis*-regulatory elements at T-cell receptor alpha locus is associated with gene expression in DLBCL. (A) Gain and loss of a CRE interacting with the *MMP14* and *PRMT5* promoters. Top panel shows position of CNVs at the CRE; with copy number gains and losses represented by solid and dashed lines respectively. Second panel shows chromatin looping interactions between the *MMP14* and *PRMT5* promoters and CREs, with the interaction between the promoters and the considered CRE colored yellow. Third panel details ChIP-seq histone mark signals in naïve B-cells. Bottom panels show positions of BRD4-bound enhancers in DLBCL[4]. CNV status at CRE and expression of (B) *MMP14* and (C) *PRMT5* in DLBCL tumors. Whilst the CREs are lost in 20 tumors, only 19

tumors are considered in the differential expression analysis, as one tumor also has a CNV at the target genes. Association between copy number status and gene expression assessed through linear regression. Boxplot hinges extend to the most extreme data points that are no more than 1.5 times the interquartile range from the box.

Figure 6: Copy number variation at *cis*-regulatory element is associated with *IGLL5* expression in B-cell malignancies. (A) The loss of a CRE interacting with the *IGLL5* promoter. Top panel shows position of CNVs at the CRE, all of which are losses, and the position of the VJ junction. Second panel shows chromatin looping interactions between the *IGLL5* promoter and CREs, with the interaction between the promoter and the considered CRE colored yellow. Third panel details ChIP-seq histone mark signals in naïve B-cells. Bottom panels shows positions of BRD4-bound enhancers in DLBCL[35]. CNV status at CRE and gene expression in (B) DLBCL and (C) FL tumors. (D) CNV status at CRE and gene expression in secondary analysis of CLL tumors. Association between copy number status and gene expression assessed through linear regression. Boxplot hinges extend to the most extreme data points that are no more than 1.5 times the interquartile range from the box.

FIGURE 1

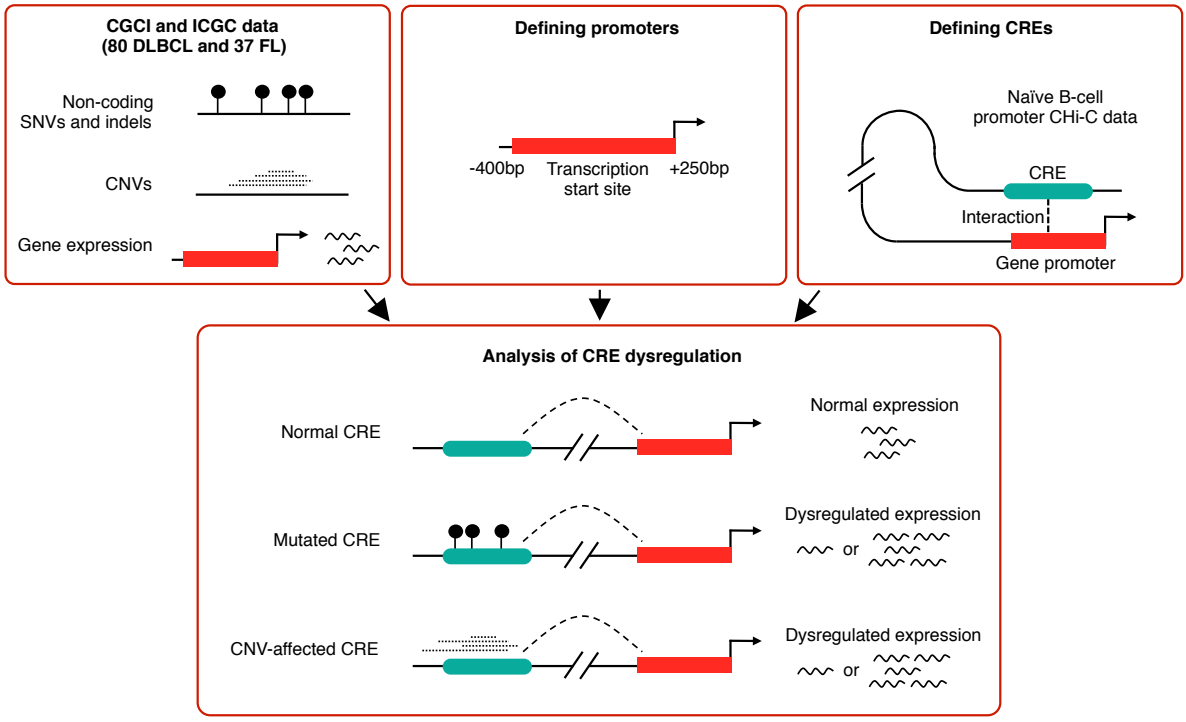
CGCI and ICGC data
(80 DLBCL and 37 FL)
Non-coding
SNVs and indels
CNVs
Gene expression
Defining promoters
-400bp
Transcription
start site
+250bp
Defining CREs
Naïve B-cell
promoter CHi-C data
CRE
Interaction
Gene promoter
Analysis of CRE dysregulation
Normal CRE
Normal expression
Mutated CRE
Dysregulated expression
or
CNV-affected CRE
Dysregulated expression
or

FIGURE 2

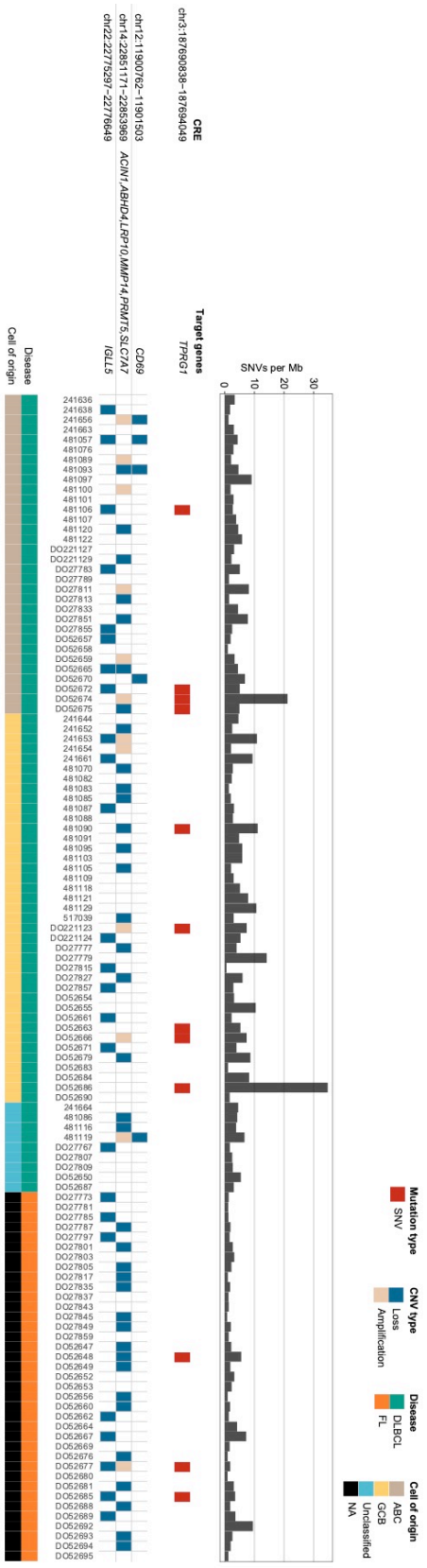
CRE
chr3:187690838–187694049
Target genes
TPRG1
SNVs per Mb
0
10
20
30
chr12:11900762–11901503
chr14:22851171–22853969
chr22:22775297–22776649
CD69
ACIN1,ABHD4,LRP10,MMP14,PRMT5,SLC7A7
IGLL5
Disease
Cell of origin
Mutation type
SNV
CNV type
Loss
Amplification
Disease
DLBCL
FL
Cell of origin
ABC
GCB
Unclassified
NA

FIGURE 3

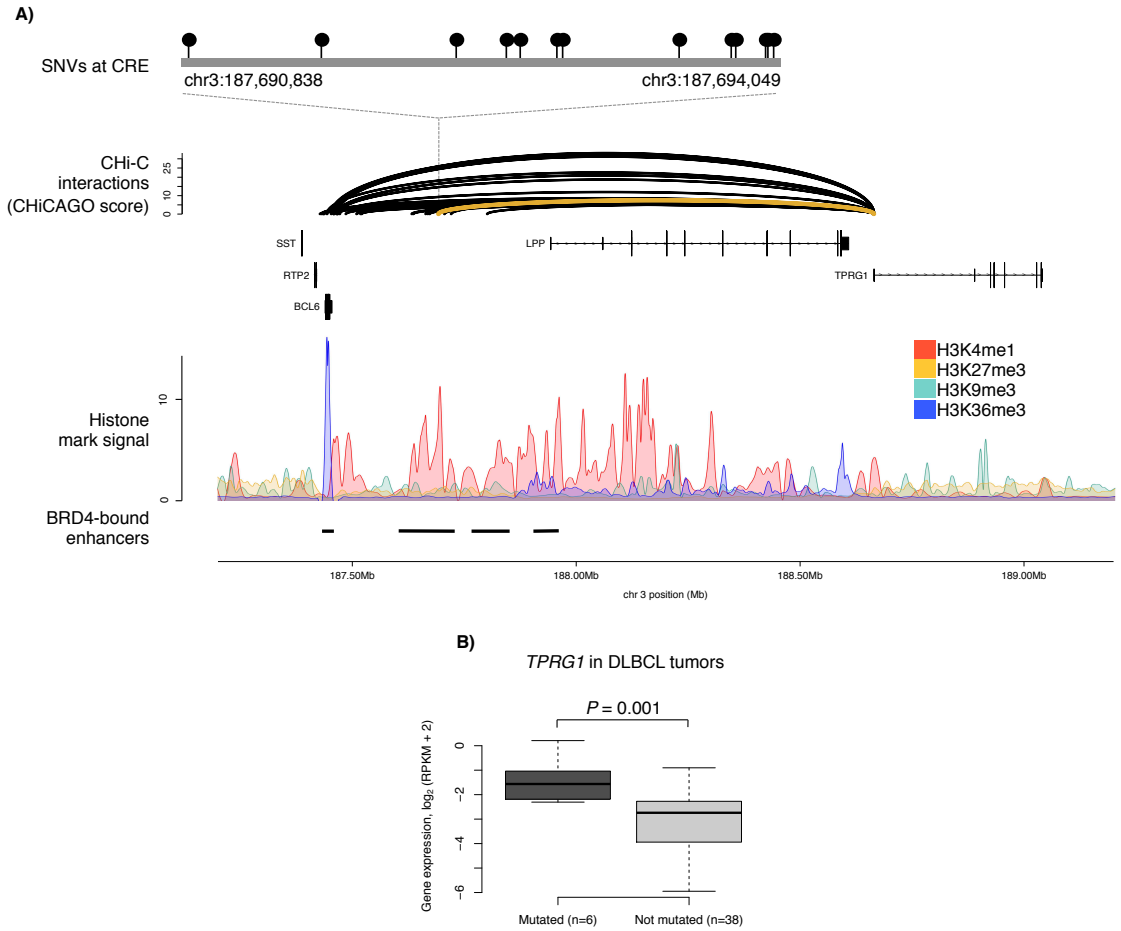
A)
SNVs at CRE
chr3:187,690,838
chr3:187,694,049
CHi-C interactions (CHiCAGO score)
0
10
25
SST
LPP
RTP2
TPRG1
BCL6
H3K4me1
H3K27me3
H3K9me3
H3K36me3
Histone mark signal
0
10
BRD4-bound enhancers
187.50Mb
188.00Mb
188.50Mb
189.00Mb
chr 3 position (Mb)
B)
TPRG1 in DLBCL tumors
P = 0.001
Gene expression, log2 (RPKM + 2)
0
−2
−4
−6
Mutated (n=6)
Not mutated (n=38)

FIGURE 4

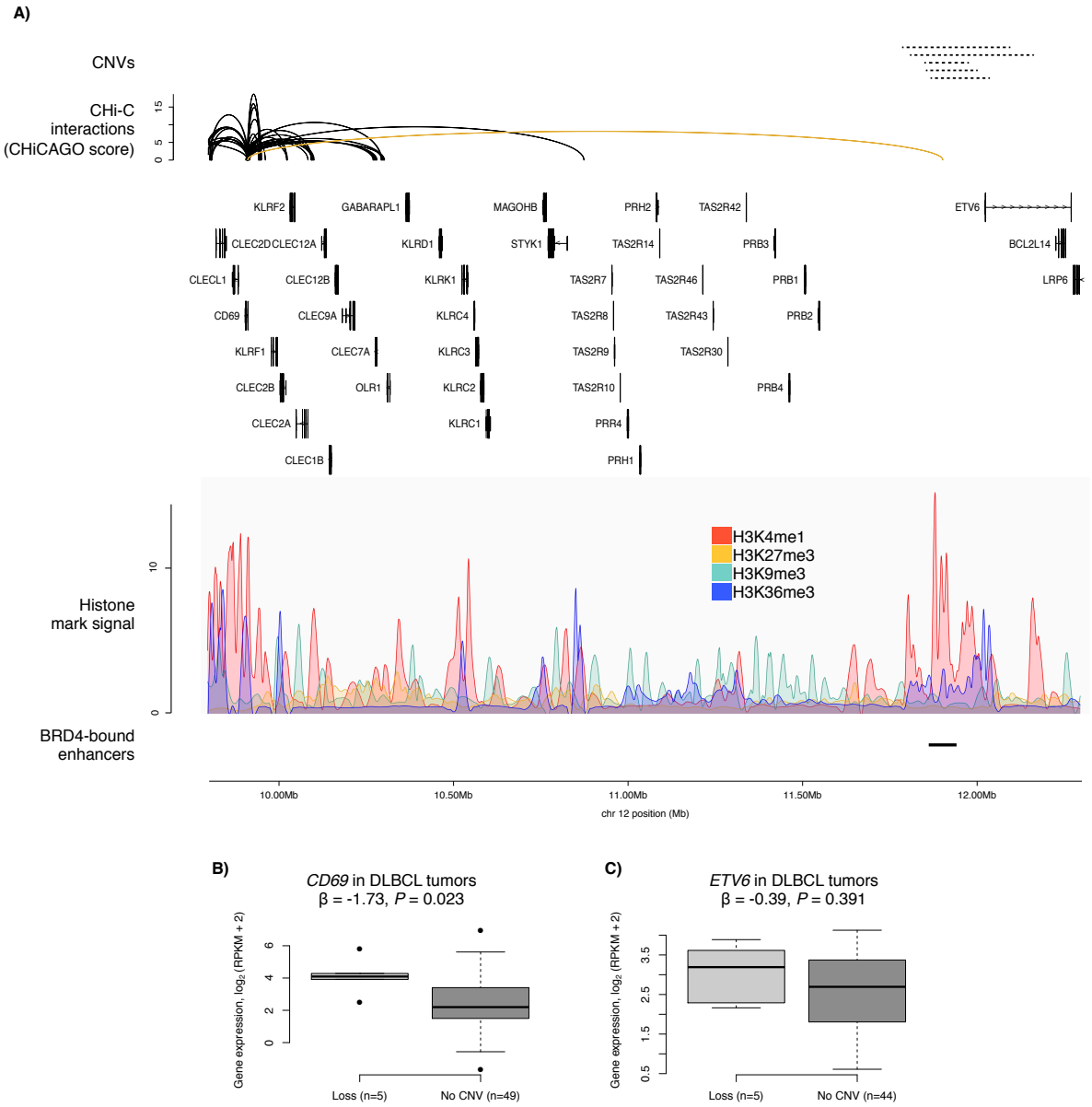
A)
CNVs
CHi-C interactions (CHiCAGO score)
0
5
15
KLRF2
GABARAPL1
MAGOHB
PRH2
TAS2R42
ETV6
CLEC2D
CLEC12A
KLRD1
STYK1
TAS2R14
PRB3
BCL2L14
CLECL1
CLEC12B
KLRK1
TAS2R7
TAS2R46
PRB1
LRP6
CD69
CLEC9A
KLRC4
TAS2R8
TAS2R43
PRB2
KLRF1
CLEC7A
KLRC3
TAS2R9
TAS2R30
CLEC2B
OLR1
KLRC2
TAS2R10
PRB4
CLEC2A
KLRC1
PRR4
CLEC1B
PRH1
Histone mark signal
0
10
H3K4me1
H3K27me3
H3K9me3
H3K36me3
BRD4-bound enhancers
10.00Mb
10.50Mb
11.00Mb
11.50Mb
12.00Mb
chr 12 position (Mb)
B)
CD69 in DLBCL tumors
β = -1.73, P = 0.023
Gene expression, log2 (RPKM + 2)
0
2
4
6
Loss (n=5)
No CNV (n=49)
C)
ETV6 in DLBCL tumors
β = -0.39, P = 0.391
Gene expression, log2 (RPKM + 2)
0.5
1.5
2.5
3.5
Loss (n=5)
No CNV (n=44)

FIGURE 5

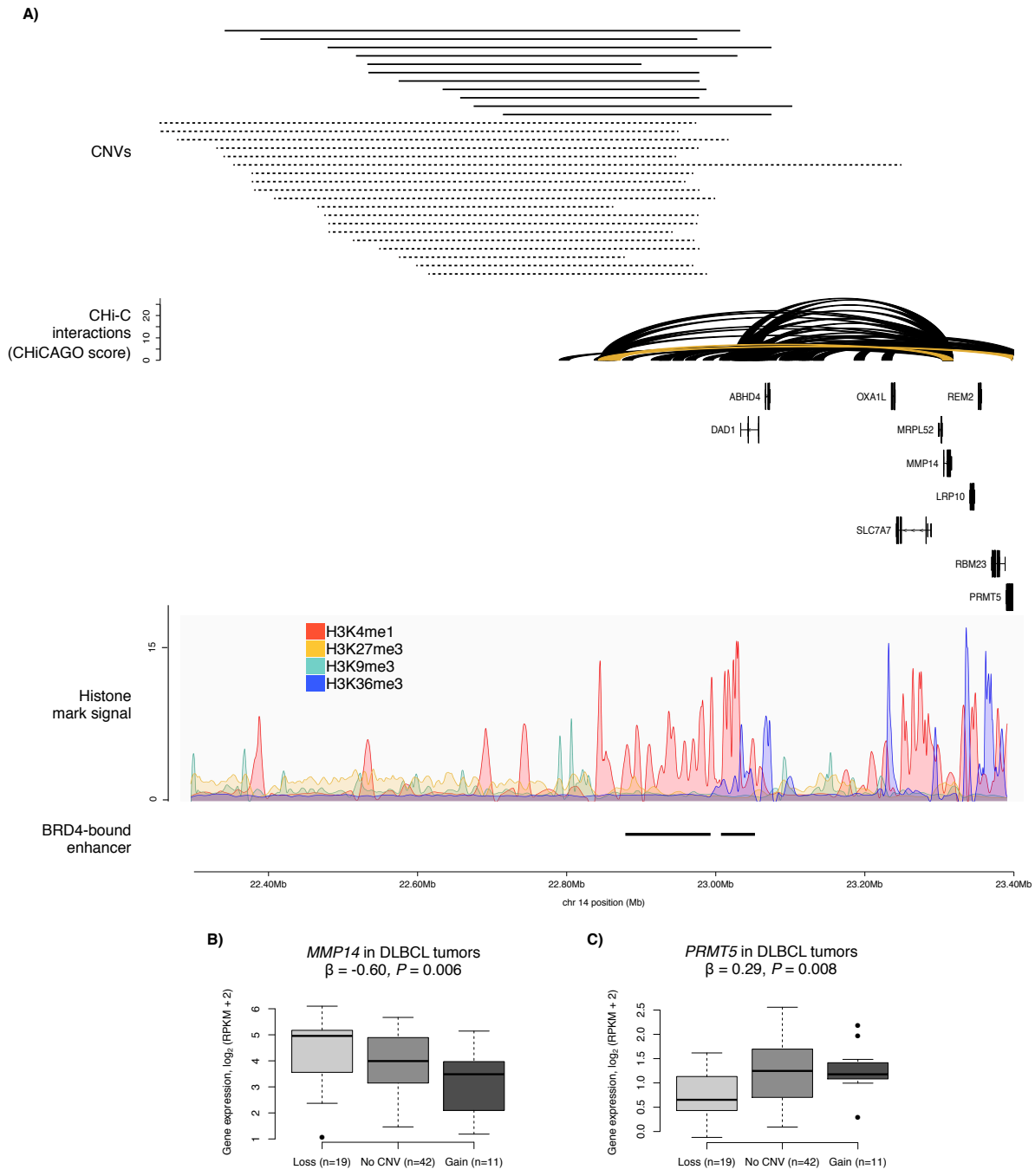
A)
CNVs
CHi-C interactions (CHiCAGO score)
0
10
20
ABHD4
OXA1L
REM2
DAD1
MRPL52
MMP14
LRP10
SLC7A7
RBM23
PRMT5
Histone mark signal
H3K4me1
H3K27me3
H3K9me3
H3K36me3
15
0
BRD4-bound enhancer
22.40Mb
22.60Mb
22.80Mb
23.00Mb
23.20Mb
23.40Mb
chr 14 position (Mb)
B)
MMP14 in DLBCL tumors
β = -0.60, P = 0.006
Gene expression, log2 (RPKM + 2)
Loss (n=19)
No CNV (n=42)
Gain (n=11)
C)
PRMT5 in DLBCL tumors
β = 0.29, P = 0.008
Gene expression, log2 (RPKM + 2)
Loss (n=19)
No CNV (n=42)
Gain (n=11)

FIGURE 6

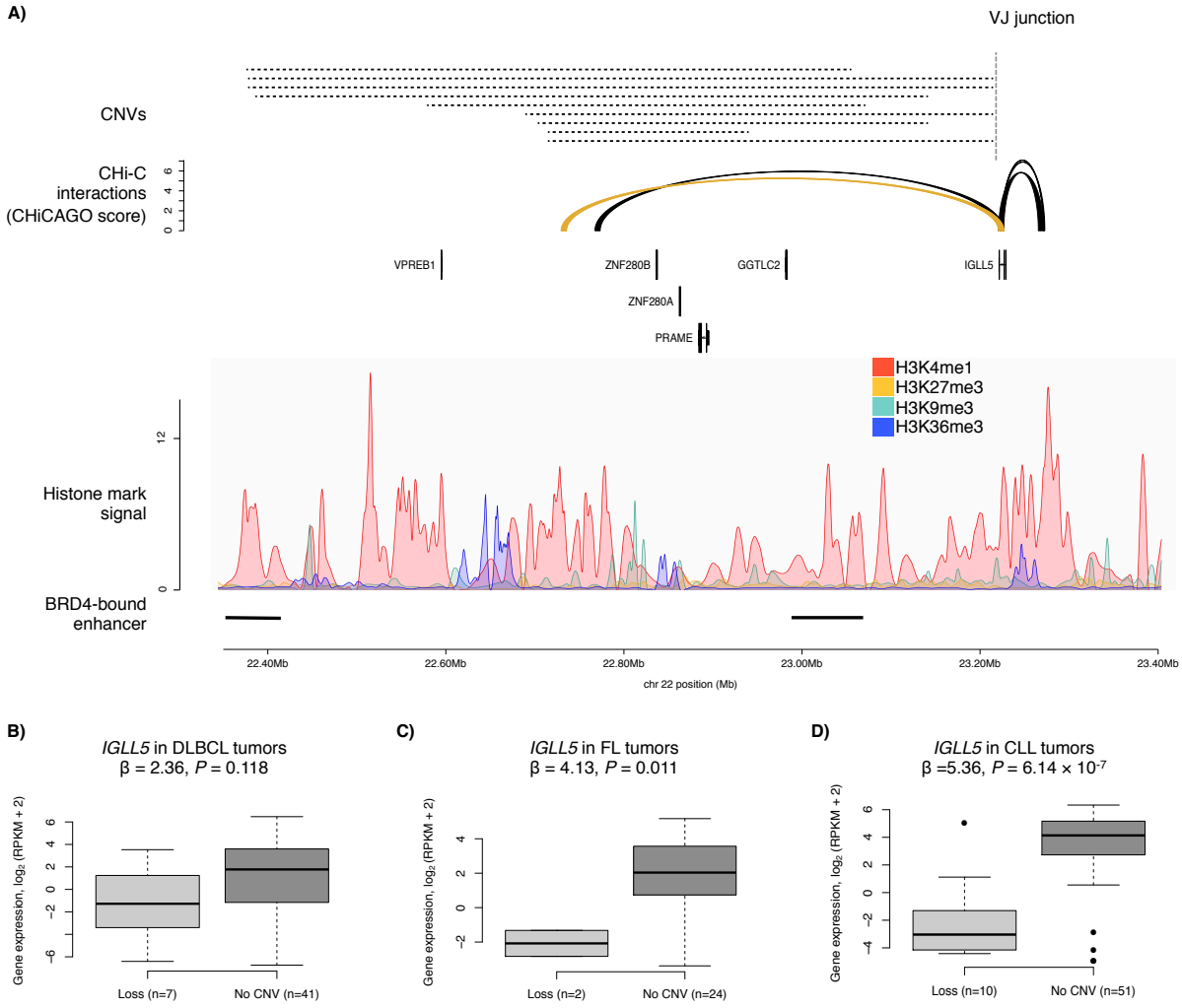
A)
VJ junction
CNVs
CHi-C interactions (CHiCAGO score)
VPREB1
ZNF280B
GGTLC2
IGLL5
ZNF280A
PRAME
H3K4me1
H3K27me3
H3K9me3
H3K36me3
Histone mark signal
BRD4-bound enhancer
22.40Mb
22.60Mb
22.80Mb
23.00Mb
23.20Mb
23.40Mb
chr 22 position (Mb)
B)
IGLL5 in DLBCL tumors
β = 2.36, P = 0.118
Gene expression, log2 (RPKM + 2)
Loss (n=7)
No CNV (n=41)
C)
IGLL5 in FL tumors
β = 4.13, P = 0.011
Loss (n=2)
No CNV (n=24)
D)
IGLL5 in CLL tumors
β =5.36, P = 6.14 × 10-7
Loss (n=10)
No CNV (n=51)

SUPPLEMENTARY METHODS

Whole genome sequencing data

WGS data from the ICGC samples were downloaded from the ICGC DCC Data Portal as tumor and matched-normal BAM files aligned to GRCh37. WGS data from the CGCI samples were downloaded from dbGaP as tumor and matched-normal unaligned FASTQ files. We aligned CGCI sample reads to the same version of GRCh37 employed in the PCAWG project, using BWA MEM[1]. Duplicate reads were marked, base quality scores recalibrated and local realignment around indels completed using GATK (v3)[2].

Calling SNVs and indels

For the ICGC samples, sets of SNVs, called using MuTect[3] with data from dbSNP v132[4] and COSMIC noncoding variants v54[5] used for additional support, were downloaded from the ICGC DCC Data Portal. For the CGCI samples, we called mutations across the whole genome using MuTect and data from the same versions of dbSNP and COSMIC. For both the ICGC and CGCI samples we used FoxoG to remove any mutations that may have been caused by oxidative DNA damage during sample preparation[6]. In addition, we ensured that variants were supported by a minimum of one alternative read in each strand direction, a mean Phred base quality score >26, mean mapping quality ≥50, and an alignability site score of 1 when using the alignability of 100mers by GEM from ENCODE. To minimize the likelihood of false positives, the Duke excluded and HiSeqDepth top 5% regions defined by UCSC Genome Browser were omitted from the analysis. Furthermore, we excluded immune system-coupled somatic hypermutation regions corresponding to 429 annotated immunoglobulin loci and the major histocompatibility complex loci (with each region extended by 50kb, as defined in Ensembl v73).

For the ICGC samples, small insertions and deletions (indels), called using Platypus[7], were downloaded from the ICGC DCC Data Portal. We also called indels for the CGCI samples using Platypus with default parameters.

Calling structural variants

For the ICGC samples, somatic CNVs called using ascatNgs[8], and translocation and inversion breakpoints called using DELLY[9], were downloaded from the ICGC DCC Data Portal. For the CGCI samples, we also called somatic CNVs using ascatNgs and translocation and inversion breakpoints using DELLY.

RNA-sequencing data

ICGC tumor sample RNA-seq data were downloaded as aligned BAM files from the ICGC DCC Data Portal. As part of the PCAWG project, reads in these files were aligned to GRCh37 using TopHat2[10] and GENCODE v19 annotated mRNA transcripts. We downloaded CGCI tumor sample RNA-seq data as unaligned FASTQ files from dbGaP and aligned reads using a pipeline identical to that used to align the ICGC sample reads. For both the ICGC and CGCI samples, we computed read counts using htseq-count and excluded genes with zero counts in >90% of tumors[11]. We applied upper-quartile normalization and computed RPKM values. Batch correction between cohorts was conducted using ComBat[12]. To avoid taking the logarithm of negative values, 2 was added to RPKM values before they were $\log_2$ transformed.

Classification of DLBCL as ABC or GCB

DLBCL tumors were assigned to ABC, GCB and Unclassified subtypes as *per* Reddy *et al.*[13]. Using this approach, 32 DLBCL tumors were classified as ABC, 39 as GCB and 9 as Unclassified.

Additional filtering of CHi-C data

We performed an additional filtering of the CHi-C data to remove regions identified as duplicated in hg38, but not hg19[14], as these may lead to the false identification of promoter-CRE interactions. To identify CREs not mapping to unique locations in hg38, hg19 was split into windows of 100bp prior to alignment to hg38 using BWA. Bases where the majority of reads containing it could be mapped elsewhere in the genome with at most one mismatch or gap were defined as poorly mapped (http://bit.ly/snpable). CREs were excluded if >5% of their constituent bases were poorly mapped.

Mutational signature analysis

Signatures reported by Alexandrov *et al.*[15] were attributed to each sample using Palimpsest with default parameters (**Table S6**)[16, 17]. Only those signatures previously observed in B-cell lymphoma and lymphoid cells were considered (SBS1, SBS2, SBS3, SBS5, SBS6, SBS9, SBS13, SBS17a, SBS17b, SBS34, SBS36, SBS37, SBS40, SBS42, SBS84 and SBS85)[15]. Mutations caused by canonical activation-induced cytidine deaminase (AID) tend to cluster in the genome[18], and we therefore classified mutations as clustered or non-clustered and attributed signatures to these mutations separately[15]. Mutations were classified as clustered if the minimum distance to all other mutations on the same chromosome in the same tumour was less than 1,000bp[18]. The numbers of clustered and non-clustered mutations associated with each signature in each tumour was then summed to calculate the overall contribution of each signature to each tumour. As per Letouzé *et al*.[16], we computed the probability that each somatic mutation occurs as a result of the process underlying each mutational signature, considering the substitution type and the overall contribution of each signature to each tumour. To assess whether each recurrently mutated promoter and CRE was enriched with mutations attributed to each signature, we compared the probability distribution of mutations in the regulatory element to the probability distribution of all other mutations observed in tumours in which the regulatory element was mutated, using a one-sided Wilcoxon rank-sum test. We consider a significance threshold of $P<0.05$ to be suggestive of signature enrichment.

RSS motif identification

We used FIMO to identify RSS sites at CNV boundaries[19], with weights for position weight matrices taken from a reported RSS conservation table[20]. For each CRE-disrupting CNV associated with differential gene expression, we scanned windows of 1kb centered on each CNV boundary called by ascatNgs, to allow for ambiguity in the exact position of the boundary. Spacer lengths of 9-13bp and 20-25bp were allowed between the motifs[21]. In **Table S13** we report those RSS sites with a space of correct length for which both motifs were identified by FIMO at a 25% FDR threshold.

Subtype analyses

For those CREs affected by mutations associated with differential target gene expression, we assessed the enrichment of DLBCL COO subtypes in the affected tumors. For each COO subtype enrichment was assessed using a two-tailed Fisher's exact test, comparing tumors from the subtype against all other tumors.

Integrated analysis of coding and non-coding mutations

The tendency of coding and non-coding mutations affecting genes to occur in different tumors was assessed using a two-tailed Fisher's exact test. Pathways significantly altered by coding and non-coding mutations in DLBCL were identified using Reactome[22], with significance thresholded at $Q<0.1$. 150 genes with recurrent coding mutations in DLBCL identified by Reddy *et al.* were included in this analysis[13].

Epigenetic annotation of regulatory regions

ChIP-seq data from naïve B cells (NC14_42), CD38-negative naïve B cells (S004KB), germinal center B cells (T14_10), unswitched memory B cells (pool_9) and class-switched memory B cells (csMBC_pool_2) for H3K4me1, H3K27me3, H3K9me3 and H3K36me3 were downloaded from BLUEPRINT. Co-ordinates were mapped from GRCh38 to GRCh37 using liftOver. BRD4-loaded enhancers, defined using ChIP-seq data from the Ly1 cell line, were obtained from Chapuy *et al.*[23], and co-ordinates mapped from NCBI36 to GRCh37 using liftOver.

REFERENCES

1. Li H. Aligning sequence reads, clone sequences and assembly contigs with BWA-MEM. *arXiv*. 2013.

2. McKenna A, et al. The Genome Analysis Toolkit: a MapReduce framework for analyzing next-generation DNA sequencing data. *Genome Res*. 2010; **20** (9): 1297-1303.

3. Cibulskis K, et al. Sensitive detection of somatic point mutations in impure and heterogeneous cancer samples. *Nat Biotechnol*. 2013; **31** (3): 213-219.

4. Sherry ST, et al. dbSNP: the NCBI database of genetic variation. *Nucleic Acids Res*. 2001; **29** (1): 308-311.

5. Forbes SA, et al. COSMIC: exploring the world's knowledge of somatic mutations in human cancer. *Nucleic Acids Res*. 2015; **43** (Database issue): D805-811.

6. Costello M, et al. Discovery and characterization of artifactual mutations in deep coverage targeted capture sequencing data due to oxidative DNA damage during sample preparation. *Nucleic Acids Res*. 2013; **41** (6): e67.

7. Rimmer A, et al. Integrating mapping-, assembly- and haplotype-based approaches for calling variants in clinical sequencing applications. *Nat Genet*. 2014; **46** (8): 912-918.

8. Raine KM, et al. ascatNgs: Identifying Somatically Acquired Copy-Number Alterations from Whole-Genome Sequencing Data. *Curr Protoc Bioinformatics*. 2016; **56** 15 19 11-15 19 17.

9. Rausch T, Zichner T, Schlattl A, Stutz AM, Benes V, Korbel JO. DELLY: structural variant discovery by integrated paired-end and split-read analysis. *Bioinformatics*. 2012; **28** (18): i333-i339.

10. Kim D, Pertea G, Trapnell C, Pimentel H, Kelley R, Salzberg SL. TopHat2: accurate alignment of transcriptomes in the presence of insertions, deletions and gene fusions. *Genome Biol*. 2013; **14** (4): R36.

11. Anders S, Pyl PT, Huber W. HTSeq--a Python framework to work with high-throughput sequencing data. *Bioinformatics*. 2015; **31** (2): 166-169.

12. Johnson WE, Li C, Rabinovic A. Adjusting batch effects in microarray expression data using empirical Bayes methods. *Biostatistics*. 2007; **8** (1): 118-127.

13. Reddy A, et al. Genetic and Functional Drivers of Diffuse Large B Cell Lymphoma. *Cell*. 2017; **171** (2): 481-494 e415.

14. Hoang PH, et al. Whole-genome sequencing of multiple myeloma reveals oncogenic pathways are targeted somatically through multiple mechanisms. *Leukemia*. 2018.

15. Alexandrov L, et al. The Repertoire of Mutational Signatures in Human Cancer. *bioRxiv*. 2018.

16. Letouze E, et al. Mutational signatures reveal the dynamic interplay of risk factors and cellular processes during liver tumorigenesis. *Nat Commun*. 2017; **8** (1): 1315.

17. Shinde J, et al. Palimpsest: an R package for studying mutational and structural variant signatures along clonal evolution in cancer. *Bioinformatics*. 2018; **34** (19): 3380-3381.

18. Kasar S, et al. Whole-genome sequencing reveals activation-induced cytidine deaminase signatures during indolent chronic lymphocytic leukaemia evolution. *Nat Commun*. 2015; **6** 8866.

19. Grant CE, Bailey Tl Fau - Noble WS, Noble WS. FIMO: scanning for occurrences of a given motif. *Bioinformatics*. 2011; **27** 1017-1018.

20. Hesse JE, Lieber MR, K. M, Gellert M. V(D)J recombination: a functional definition of the joining signals. *Genes and Development*. 1989; **3** (7): 1053-1061.

21. Papaemmanuil E, et al. RAG-mediated recombination is the predominant driver of oncogenic rearrangement in ETV6-RUNX1 acute lymphoblastic leukemia. *Nature Genetics*. 2014; **42** (2): 116-125.

22. Croft D, et al. Reactome: a database of reactions, pathways and biological processes. *Nucleic Acids Res*. 2011; **39** (Database issue): D691-697.

23. Chapuy B, et al. Discovery and characterization of super-enhancer-associated dependencies in diffuse large B cell lymphoma. *Cancer Cell*. 2013; **24** (6): 777-790.

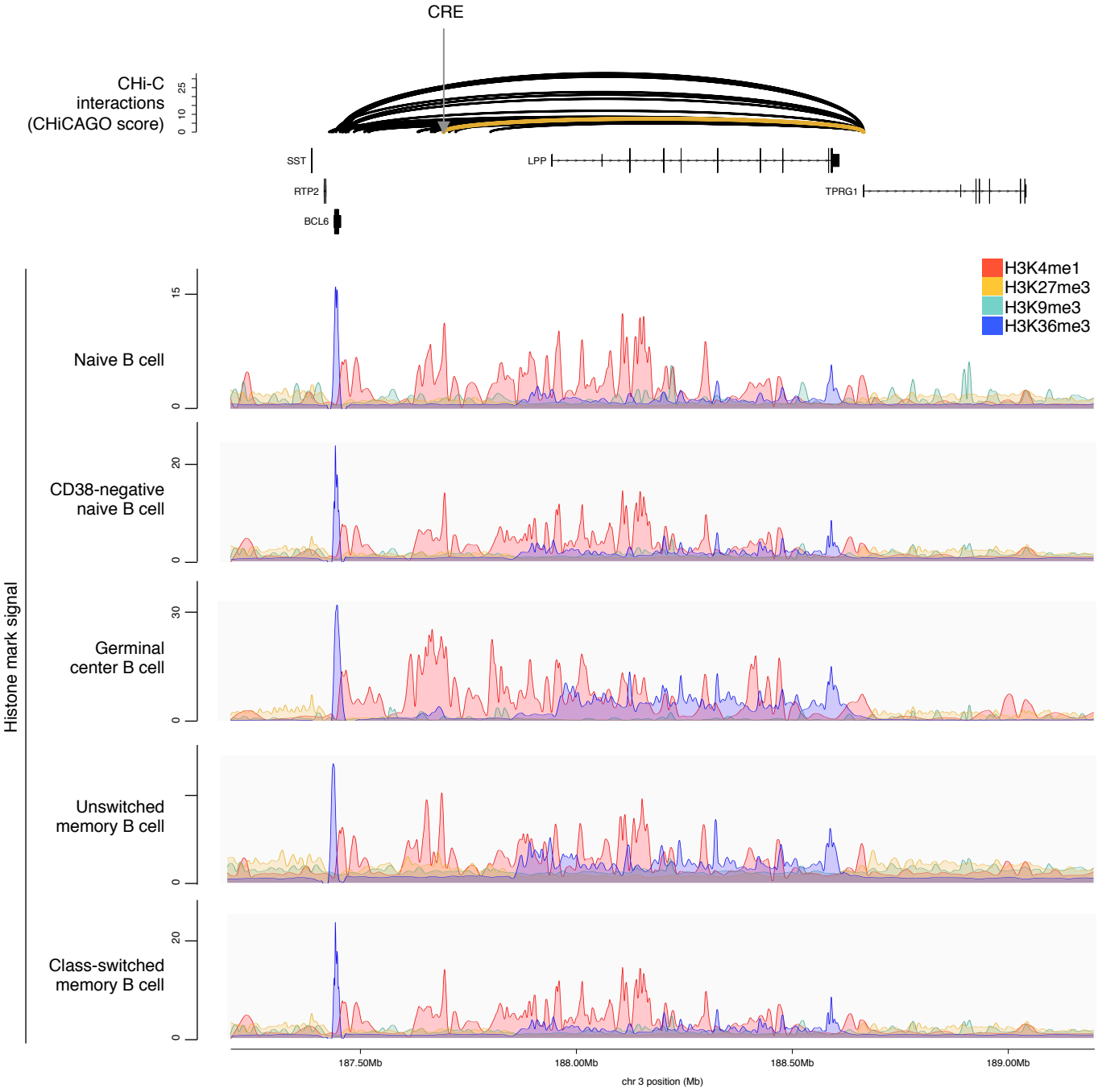

Figure S1: SNVs at a CRE interacting with the *TPRG1* promoter. Top panel shows position of the CRE. Second panel shows chromatin looping interactions between the *TPRG1* promoter and CREs, with the interaction between the promoter and the SNV-disrupted CRE colored yellow. Lower panels detail ChIP-seq histone mark signals in B cells at different differentiation stages.

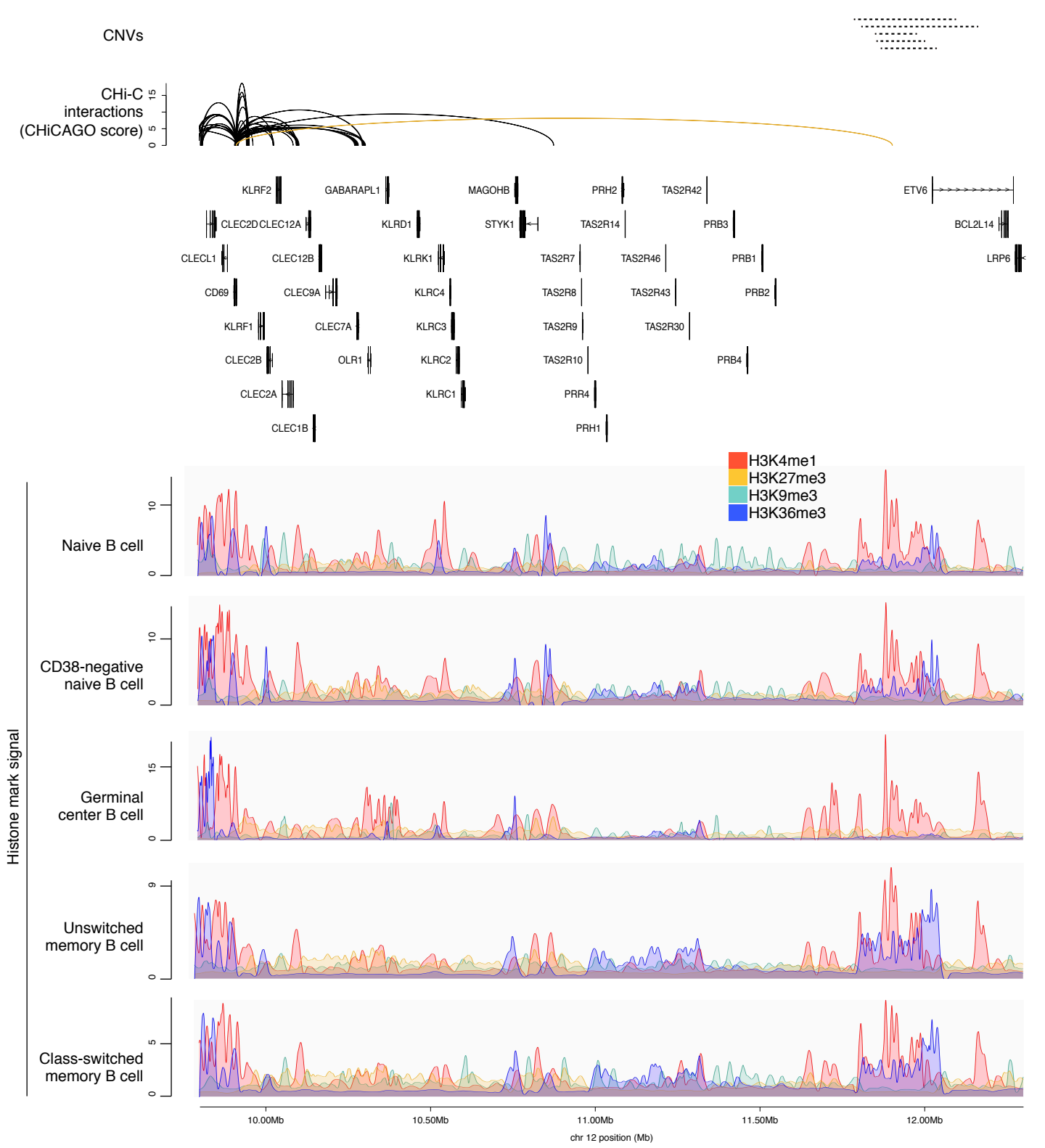

Figure S2. Loss of a CRE interacting with the *CD69* promoter. Top panel shows position of CNVs at the CRE, all of which are copy number losses. Second panel shows chromatin looping interactions between the *CD69* promoter and CREs, with the interaction between the promoter and the CNV-disrupted CRE colored yellow. Lower panels detail ChIP-seq histone mark signals in B cells at different differentiation stages.

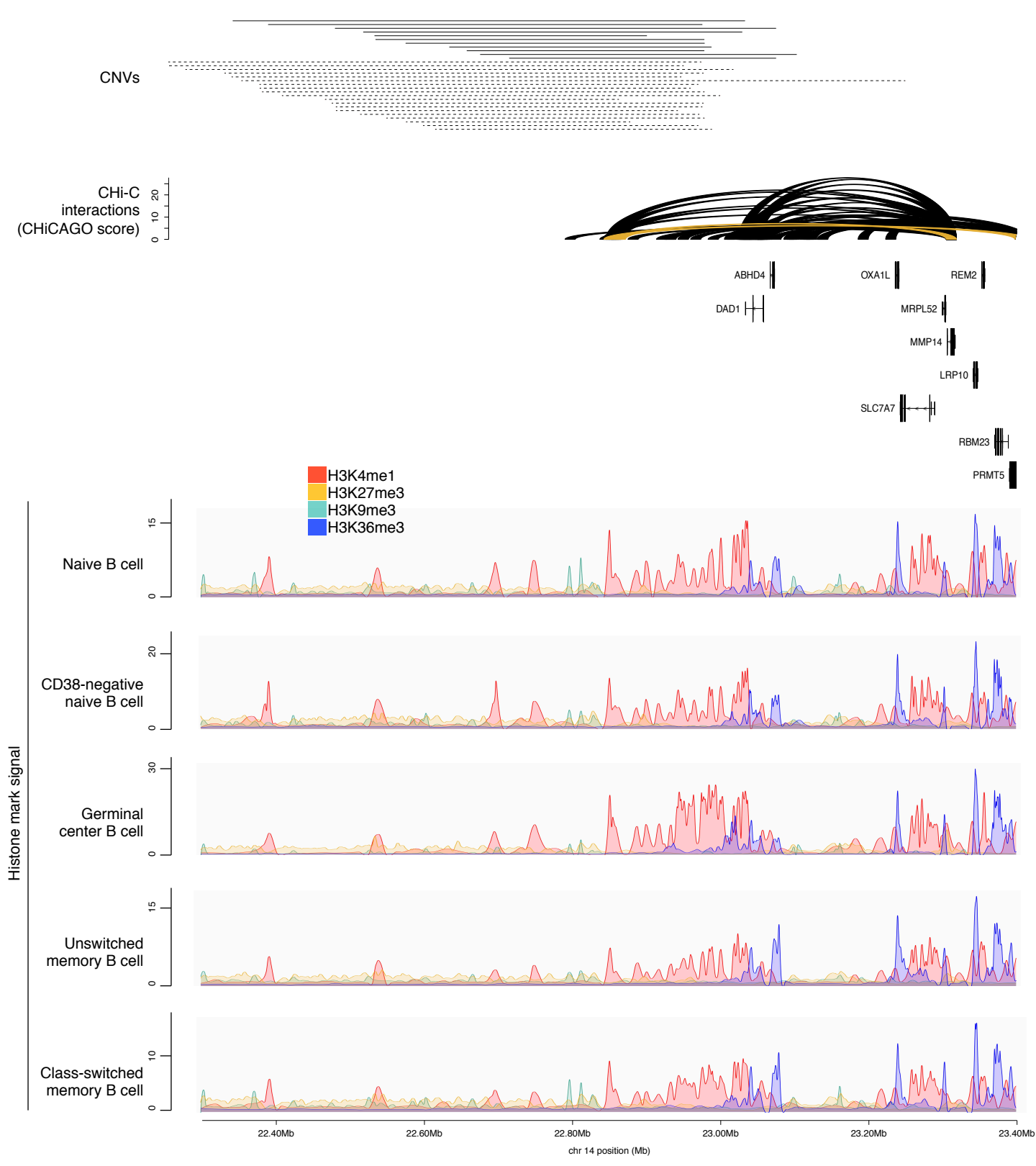

Figure S3. Gain and loss of a CRE interacting with the *MMP14* and *PRMT5* promoters. Top panel shows position of CNVs at the CRE; with copy number gains and losses represented by solid and dashed lines respectively. Second panel shows chromatin looping interactions between the *MMP14* and *PRMT5* promoters and CREs, with the interaction between the promoters and the considered CRE colored yellow. Lower panels detail ChIP-seq histone mark signals in B cells at different differentiation stages.

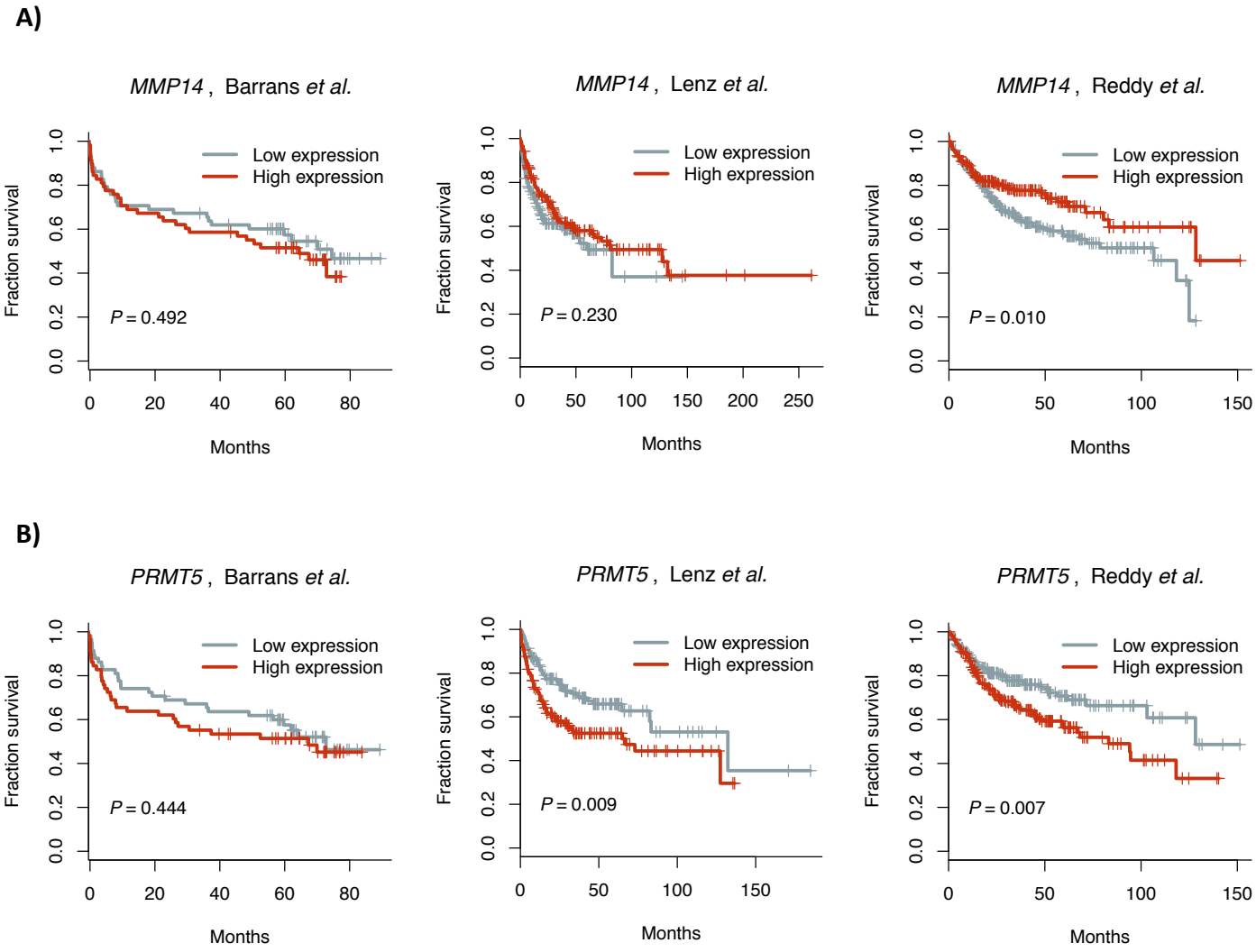

Figure S4. Kaplan-Meier survival analysis of (A) *MMP14* and (B) *PRMT5* expression (the two genes with expression significantly associated with survival in the Cox proportional hazards model analysis) in data sets from Barrans *et al.* (*n*=115), Lenz *et al.* (*n*=276) and Reddy *et al.* (n=*404*). Distribution differences assessed using the log-rank test.

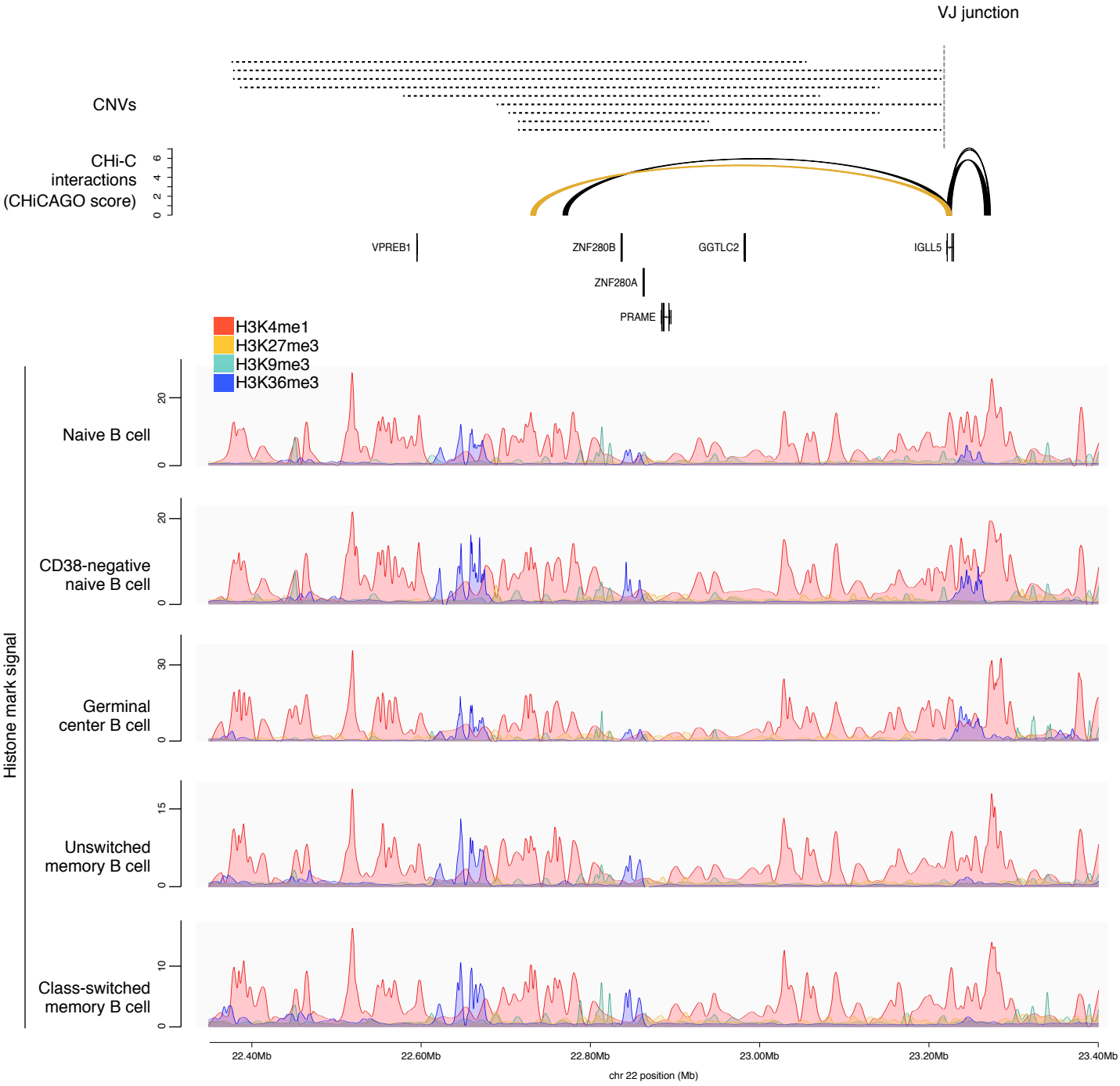

Figure S5. Loss of a CRE interacting with the *IGLL5* promoter. Top panel shows position of CNVs at the CRE, all of which are losses, and the position of the VJ junction. Second panel shows chromatin looping interactions between the *IGLL5* promoter and CREs, with the interaction between the promoter and the considered CRE colored yellow. Lower panels detail ChIP-seq histone mark signals in B cells at different differentiation stages.